Safe Data-Driven Secondary Control of Distributed Energy Resources

Madi Zholbaryssov and Alejandro D. Domínguez-García, *Senior Member, IEEE*

Abstract—In this paper, we present a data-driven secondary controller for regulating to some desired values several state variables of interest in an inverter-based power system, namely, electrical frequency, voltage magnitudes at critical buses, and active power flows through critical lines. The secondary controller is based on online feedback optimization, leveraging the learned sensitivities of changes in the state variables to changes in inverter active and reactive power setpoints. To learn the sensitivities accurately from data, the feedback optimization has a built-in mechanism for keeping the secondary control inputs persistently exciting without degrading its performance or compromising system operational reliability. To ensure safe and reliable operation, we present an approach based on Gaussian process regression that, by making an inference about the modeling uncertainties not accounted for in the sensitivity-based prediction model, allows the controller to correct the predictions and find safe control actions, for which the prediction errors are more likely to be small. The feedback optimization also utilizes the learned power-voltage characteristics of photovoltaic (PV) arrays to compute DC-link voltage setpoints so as to allow the PV arrays to track the power setpoints. To learn the power-voltage characteristics, we separately execute a data-driven approach that fits a concave polynomial to the collected power-voltage measurements by solving a sum-of-squares (SoS) optimization. We showcase the secondary controller using the modified IEEE-14 bus test system, in which conventional energy sources are replaced with inverter-interfaced DERs.

Index Terms—Power system control, data-driven control, online feedback optimization, xwdistributed energy resources, sensitivity estimation, Gaussian process regression, stochastic program.

I. INTRODUCTION

WITH the increased installation of smart meters and other measurement devices in power distribution systems, there is a growing impetus for designing cost-effective and reliable control methods that harness the full potential of the data gathered by such measurement devices. However, at least in the foreseeable future, substantial parts of distribution systems will lack measurement devices and suitable communication infrastructure, making the identification of accurate models for distribution systems a hard problem. The lack of accurate models poses major challenges to large-scale integration and coordination of renewable generation in distribution systems, motivating the development of data-driven approaches for their coordination that does not assume any prior knowledge of the underlying power system model [1]. Moreover, to achieve the ultimate goal of replacing conventional fossil fuel-based energy sources with renewable energy sources (RESs), intermittency of their power output must be considered in the control system design, e.g., by endowing RESs with fast frequency and voltage regulation capabilities. Availability of data and recent advances in the area of data-driven decision-making (see, e.g, [2], [3]) offer us new opportunities and tools for dealing with uncertainty associated with the power produced by RESs.

Despite the recent success of data-driven techniques in solving various control problems that arise in power systems (see, e.g., [4]–[17]), there exist a number of issues that might limit their practicality. Good performance of such techniques depends on extensive exploration of the control action space, which increases the risk of taking a sequence of unsafe control actions that might be detrimental to safe and reliable operation of the target system. The problem of devising a strategy that allows data-driven controllers to persistently excite control inputs without degrading their performance or compromising safety of the system is largely neglected in the literature.

A vast body of data-driven techniques for power systems control and operation have recently been developed in the literature (see, e.g., [4]–[17]). Linear system identification techniques were applied in [4], [5], [6], [9] to learn linear sensitivities of various state variables to control inputs and in [11] to learn topology and line parameters of radial power distribution systems for performing different control tasks. For example, the authors of [9] use the learned sensitivities for regulating the active power exchange between a power distribution system and the bulk grid to which it is interconnected. The authors of [11] propose a data-driven voltage regulation approach based on the estimated topology and line parameters of radial power distribution systems. A number of works (see, e.g., [8], [12]) proposed data-driven approaches that use measurement data to directly perform controller synthesis without system identification. For example, the authors of [8] propose a data-driven frequency control method that uses the datasets generated by the linear quadratic regulator (LQR) to learn a static feedback gain viable for various amounts of inertia present in the system. The authors of [12] propose a data-driven H_2 optimization that directly uses measurements for synthesis of primary and secondary controllers. Another body of works (see, e.g., [7],

[13], [14]) utilized emerging machine learning techniques, e.g., deep learning, and deep reinforcement learning, to make control decisions relying on deep neural networks for modeling the relevant underlying physics of power systems; however, training deep neural networks requires large volumes of data.

In this paper, we propose a data-driven secondary controller for an inverter-based power system, the objective of which is to regulate to some desired values several variables of interest, namely, the electrical frequency across the system, voltage magnitudes at critical buses, and active power flows through critical lines. The design of the secondary controller is based on online feedback optimization that makes use of learned sensitivities of changes in the variables to be regulated to changes in the control inputs, comprising the active and reactive power setpoints of the inverters. Compared to the existing learning-based control approaches proposed in [6], [7], [15]–[17], one of the novelties of our approach is to ensure safe and reliable operation of the system by making an additional Bayesian inference about the modeling residuals (errors), not accounted for in the sensitivity-based prediction model. This enables the controller to find safe control actions, for which accurate predictions can be made with a high degree of confidence.

Another issue neglected in recent works [6], [7], [15]–[17] that we attempt to address lies in maintaining persistent excitation of the control inputs for preventing the loss of identifiability of the sensitivities in a way less detrimental to safe and reliable operation, and control performance. A common strategy to maintain the excitation is to add a random signal without considering safety criteria related to maintaining operational reliability [9], [18]. In this work, we present a safer and more optimal approach that exploits the natural excitation of the output error due to, e.g., load fluctuations, and the learned posterior distribution of the residuals associated with the candidate control inputs, enabling us to choose safe control inputs of sufficient excitation level. Applying safe as well as persistently exciting control actions allows us to control the system in a safer and efficient manner.

An additional feature of the proposed secondary controller is to enable PV arrays to provide regulation services. One of the challenges here is to compute the power setpoints that are trackable by the PV arrays given the fluctuations in their power-voltage characteristics due to changes in solar irradiance. In this work, we attempt to integrate the learned power-voltage characteristics of the PV arrays into the proposed feedback optimization, and compute the DC-link voltage setpoints in addition to the power setpoints. In other words, the feedback optimization combines the standard secondary control objectives with the PV power tracking objectives. Meanwhile, the power-voltage characteristics are modeled by a concave polynomial fit to the collected measurements by solving a SoS optimization [19].

The remainder of this paper is organized as follows. Section II describes the adopted model of an inverter-based power system and the approach for estimating the power-voltage characteristics of PV arrays, and formulates the secondary control problem. Section III presents the sensitivity-based prediction and Gaussian process-based residual prediction models utilized by the cautious data-driven secondary controller, which is presented in Section IV. Section V provides the numerical results for the proposed controller. Concluding remarks are presented in Section VI.

II. PRELIMINARIES

In this section, we describe the adopted models of the power network and inverter-interfaced DERs, and formulate the secondary control problem under uncertainty in photovoltaic generation.

A. Power Network

We consider a collection of inverter-interfaced DERs and loads physically interconnected by an electrical network operating in balanced three-phase regime. Assume the network has N buses indexed by the elements in the set $\mathcal{V} = \{1, 2, \ldots, N\}$. Assume the network has n inverter-interfaced DERs indexed by the elements in the set $\mathcal{V}^{(g)} = \{1, 2, \ldots, n\}$. Let $\mathcal{V}_{pv} \subseteq \mathcal{V}^{(g)}$ denote the set of PV arrays interfaced with grid-following (GFL) inverters; in the remainder, we refer to these as solar inverters. The remaining DERs from the set $\mathcal{V}^{(I)} := \mathcal{V}^{(g)} \setminus \mathcal{V}_{pv}$ are assumed to be interfaced with three-phase grid-forming (GFM) inverters.

Let $\theta_i(t)$ and $V_i(t)$ respectively denote the phase and magnitude of the phasor associated with the voltage at bus i at time t. Let $\omega_i(t) := \frac{d\theta_i(t)}{dt}$ denote the local frequency at bus i at time t. Let V_i^* denote the nominal value of the magnitude of the phasor associated with the voltage at bus i, and let ω^* denote the system nominal frequency. Let $\omega(t) := \frac{1}{n}\sum_{i \in \mathcal{V}} \omega_i(t)$ denote the average frequency, which is to be regulated by the secondary controller to the nominal value, ω^*. Let $\mathcal{B}$ denote a set indexing certain critical buses, at which the voltage magnitudes are to be regulated to their respective nominal values. Define $V(t) := [\{V_i(t)\}_{i \in \mathcal{B}}]^\top$ and $V^* := [\{V_i^*\}_{i \in \mathcal{B}}]^\top$. Let $\mathcal{T}$ denote a set indexing certain critical lines, e.g., tie lines, in which the active power flows are to be regulated to their respective nominal values. Let $(i, j) \in \mathcal{T}$ denote an electrical line connecting buses i and j, $p_{ij}(t)$ denote the amount of active power that flows from bus i to bus j through line (i, j), and p_{ij}^* denote the corresponding nominal value. Define $p(t) := [\{p_{ij}(t)\}_{(i,j)\in\mathcal{T}}]^\top$ and $p^* := [\{p_{ij}^*\}_{(i,j)\in\mathcal{T}}]^\top$.

B. Inverter Models

In this work, three-phase GFM inverters are controlled using the following primary voltage and frequency droop-like control laws based on the dynamics of the so-called Andronov-Hopf oscillator [20]:

$$\dot{E}_j(t) = \frac{\xi_j}{\kappa_{j,v}^2} E_j(t) \left(2E_j^{*2} - 2E_j(t)^2\right)$$
$$- \frac{\kappa_{j,v}\kappa_{j,i}}{3C_j E_j(t)} \left(Q_j(t) - Q_j^r(t)\right), \tag{1a}$$

$$\dot{\delta}_j(t) = \omega^* - \frac{\kappa_{j,v}\kappa_{j,i}}{3C_j E_j(t)^2} \left(P_j(t) - P_j^r(t)\right), \; j \in \mathcal{V}^{(I)}, \tag{1b}$$

where $\delta_j(t)$ and $E_j(t)$ respectively denote the phase and magnitude of the phasor associated with the terminal voltage of the GFM inverter $j \in \mathcal{V}^{(I)}$ at time t, E_j^* denotes the nominal inverter voltage, ξ_j, $\kappa_{j,i}$, $\kappa_{j,v}$, and C_j are constants, $P_j(t)$ and $Q_j(t)$ denote the active and reactive power injected into the network at time t by the inverter, $P_j^r(t)$ and $Q_j^r(t)$ denote the active and

reactive power setpoints provided to the inverter at time t by the secondary controller.

At time t inverter $j \in \mathcal{V}_{pv}$ is capable of regulating its active and reactive power outputs, denoted by $P_j(t)$ and $Q_j(t)$, respectively, to the corresponding active and reactive power setpoints denoted by $P_j^r(t)$ and $Q_j^r(t)$, provided that $P_j^r(t)$ does not exceed the active power capacity of the PV array. If $P_j^r(t)$ exceeds the active power capacity, then, the inverter is assumed to provide the maximum available active power.

C. PV Power Tracking Mechanism

To extract a desired amount of power from a PV array $i \in \mathcal{V}_{pv}$, as specified by the secondary control setpoints, a certain voltage, denoted by v_i, must be applied across its terminals, as determined by the power-voltage characteristic. Hence, there is a need for a mechanism capable of converting the power setpoints computed by the secondary controller into the voltage setpoints tracked by the DC-side controller. On the other hand, the secondary controller must take into account the power-voltage characteristics of the PV arrays to ensure that the computed power setpoints are trackable by the solar inverters without exceeding the maximum active power capacity of the PV arrays.

A main challenge in designing such mechanism lies in dealing with the uncertainty of the power-voltage characteristics of the PV arrays. However, as shown in [19] and described next, these power-voltage characteristics can be accurately modeled by a degree-d polynomial fitted to the collected power-voltage measurements. Let $v_i(t)$ and $p_i(t)$ respectively denote the voltage applied across the terminals of the PV array associated with GFL $i \in \mathcal{V}_{pv}$ and the resulting active power output at time t. Then, we can write a polynomial for predicting the active power output of the PV array for a given terminal voltage v_i as follows:

$$c_i(v_i, \beta^{(i)}[k]) = \sum_{l=0}^{d} \beta_l^{(i)}[k] v_i^l. \tag{2}$$

The coefficients of the polynomial, $\beta^{(i)}[k] = [\beta_0^{(i)}[k], \beta_2^{(i)}[k], \ldots, \beta_d^{(i)}[k]]^\top$, are estimated at time instant t_k by fitting the model to the power-voltage measurements, $\{(v_i[l], p_i[l])\}_{l=k-w}^{k}$, collected over a time window denoted by w, where $v_i[l] := v_i(t_l)$ and $p_i[l] := p_i(t_l)$. The model fitting amounts to solving a linear regression problem with the additional constraints to ensure that the resulting polynomial is concave [19].

D. Control Objectives

Let $\{t_k\}_{k \geq 1}$ denote the sequence of time instants at which $P_j^r(t)$ and $Q_j^r(t)$, $j \in \mathcal{V}^{(g)}$, are adjusted. Define $P^r[k] := [P_1^r[k], P_2^r[k], \ldots, P_n^r[k]]^\top$, and $Q^r[k] := [Q_1^r[k], Q_2^r[k], \ldots, Q_n^r[k]]^\top$, where $P_j^r[k] := P_j^r(t_k)$ and $Q_j^r[k] := Q_j^r(t_k)$, and let $u[k] := [P^r[k]^\top, Q^r[k]^\top]^\top$. Then, our goal is to develop a secondary controller that regulates the output of the system, $y(t) := [\omega(t), V(t)^\top, p(t)^\top]^\top$, to the nominal level, denoted by $y^* := [\omega^*, V^{*\top}, p^{*\top}]^\top$, by adjusting the secondary control inputs, $u[k]$, while taking into account the learned power-voltage characteristics of the PV arrays as described by (2).

III. SYSTEM OUTPUT PREDICTION MODEL

In this section, we present the models for predicting the changes in the system output given the changes in the secondary control inputs. The model will later be used by the secondary controller (to be presented in Section IV).

A. Online Sensitivity Estimator

Let $\{t_k^-\}_{k \geq 1}$ denote the sequence of time instants such that $t_{k-1} < t_k^- < t_k$, $\forall k$, at which the output $y(t)$ is measured. Let $y[k] := [\omega[k], V[k]^\top, p[k]^\top]^\top$ denote the measurement of the output $y(t) = [\omega(t), V(t)^\top, p(t)^\top]^\top$ at time $t = t_{k+1}^-$, where $\omega[k] := \omega(t_{k+1}^-)$, $V[k] := [\{V_i[k]\}_{i \in \mathcal{B}}]^\top$, with $V_j[k] := V_j(t_{k+1}^-)$, and $p[k] := [\{p_{ij}[k]\}_{(i,j) \in \mathcal{T}}]^\top$, with $p_{ij}[k] := p_{ij}(t_{k+1}^-)$. Define $\Delta P^r[k] := P^r[k] - P^r[k-1]$, $\Delta Q^r[k] := Q^r[k] - Q^r[k-1]$, and let $\Delta u[k] := [\Delta P^r[k]^\top, \Delta Q^r[k]^\top]^\top$ denote the vector of the changes in the secondary control inputs producing the changes in the output denoted by $\Delta y[k] := y[k] - y[k-1]$. Here, $y[k]$ can be expressed in terms of some nonlinear function $h : \mathbb{R}^{n_u} \to \mathbb{R}^{n_y}$, $n_u := \dim(u)$, $n_y := \dim(y)$, as follows:

$$y[k] = h(u[k], \xi[k]), \tag{3}$$

where $\xi[k] := \xi(t_k)$, with $\xi(t) \in \mathbb{R}^{n_y}$ denoting some exogenous disturbance associated with changes in electrical loads and power network parameters. Then, by using the Taylor series expansion, and keeping only the linear term, we obtain that

$$\Delta y[k] = S[k] \Delta u[k] + \epsilon[k], \tag{4}$$

where $S[k] := \frac{\partial h(u[k-1], \xi[k-1])}{\partial u}$ is referred to as the sensitivity matrix, $\epsilon[k]$ represents the nonlinear terms and disturbance effects.

Consider the following linear prediction model:

$$\widehat{\Delta y}[k] = \widehat{S}[k] \Delta u[k], \tag{5}$$

where $\widehat{\Delta y}[k]$ is the estimate of $\Delta y[k]$, and $\widehat{S}[k]$ denotes the estimate of the sensitivity matrix $S[k]$, which is obtained using the method of regularized least squares as follows:

$$\widehat{S}[k+1] = \underset{S}{\operatorname{argmin}} \ \ell(S), \tag{6}$$

where

$$\ell(S) := \sum_{l=1}^{k} \lambda^{k-l} \big\| \Delta y[l] - S \Delta u[l] \big\|_2^2 + \gamma \sum_i \sum_j S_{ij}^2,$$

$\gamma > 0$ is a regularization parameter, $\lambda \in (0, 1)$ denotes the forgetting factor that allows the estimator to assign exponentially less weight to older measurements and adapt to changes in operating conditions. The regularization is introduced to reduce the sensitivity of the linear model to small variations in the collected data and increase its robustness against insufficient control input excitation at the expense of increased bias. The solution to the least-squares problem (6) can be derived as follows. We first compute the gradient of the loss function $\ell(S)$ in (6) as follows:

$$\nabla \ell(S) = -2 \sum_{l=1}^{k} \lambda^{k-l} \left(\Delta y[l] - S \Delta u[l] \right) \Delta u[l]^\top + 2\gamma S. \tag{7}$$

Then, we equate the gradient (7) to zero and obtain

$$\sum_{l=1}^{k} \lambda^{k-l} \Delta y[l] \Delta u[l]^{\top} = S \left(\sum_{l=1}^{k} \lambda^{k-l} \Delta u[l] \Delta u[l]^{\top} + \gamma I \right). \tag{8}$$

By solving (8) for S, we obtain $\widehat{S}[k+1]$:

$$\widehat{S}[k+1] = \left(\sum_{l=1}^{k} \lambda^{k-l} \Delta y[l] \Delta u[l]^{\top} \right)$$
$$\times \left(\sum_{l=1}^{k} \lambda^{k-l} \Delta u[l] \Delta u[l]^{\top} + \gamma I \right)^{-1}, \tag{9}$$

which can be written more compactly as:

$$\widehat{S}[k+1] = Y[k]^{\top} \Lambda[k] X[k] \left(X[k]^{\top} \Lambda[k] X[k] + \gamma I \right)^{-1}, \tag{10}$$

where

$$X[k] = \begin{bmatrix} \Delta u[1]^{\top} \\ \Delta u[2]^{\top} \\ \vdots \\ \Delta u[k]^{\top} \end{bmatrix}, \ Y[k] = \begin{bmatrix} \Delta y[1]^{\top} \\ \Delta y[2]^{\top} \\ \vdots \\ \Delta y[k]^{\top} \end{bmatrix}, \tag{11}$$

and $\Lambda[k]$ is a $(k \times k)$-dimensional diagonal matrix with $\Lambda_{ii}[k] = \lambda^{k-i}$. In order to accurately identify the sensitivities, we need to ensure that the applied setpoint increments, $\Delta u[t], t = 1, 2, \ldots,$ are persistently exciting.[1]

B. Inference of Modeling Residuals for Safe Control

One of the main challenges in ensuring safe and reliable operation of the system lies in finding control actions for which accurate predictions can be made with a high degree of confidence, even in the aftermath of unexpected large changes in operating conditions or the loss of identifiability of the sensitivities due to feedback control. During such events predictions can become noticeably inaccurate, in spite of the fast tracking capabilities of the linear predictor. To mitigate these issues, we present an approach that allows us to quantify a degree of confidence in the predictions by making an inference about the modeling residuals given as follows:

$$r[k] = \Delta y[k] - \hat{S}[k] \Delta u[k], \tag{12}$$

capturing nonlinear terms and disturbance effects as described by $\epsilon[k]$ in (4), and additional residual terms due to errors in the sensitivity estimates. We model each i-th component of the residual r, denoted by r_i, using a Gaussian random process defined by a mean function $m_i : \mathbb{R}^{n_u} \to \mathbb{R}$ and covariance function $K_i : \mathbb{R}^{n_u} \times \mathbb{R}^{n_u} \to \mathbb{R}$ such that the value of r_i at $\Delta u[k]$ is represented as a Gaussian random variable, i.e.,

$$r_i[k] \sim \mathcal{N} \left(m_i(\Delta u[k]), K_i(\Delta u[k], \Delta u[k]) \right). \tag{13}$$

[1] A discrete-time signal $x[t], t = 1, 2, \ldots,$ is persistently exciting if, for every k, there exist an integer l and constants $\varrho_1, \varrho_2 > 0$ such that the matrices $\varrho_1 I - \sum_{t=k}^{k+l} x[t] x[t]^{\top}$ and $\sum_{t=k}^{k+l} x[t] x[t]^{\top} - \varrho_2 I$ are positive definite [18].

Notice that the index set of a Gaussian process is typically the set of time instants, whereas, here, it is the set of possible setpoint increments. The prior distribution (13) essentially sets the properties of the candidate functions considered for inference [21]. As we collect data, the posterior distribution of the candidate functions changes to be consistent with the data, allowing us to refine our predictions. Clearly, the choice of the covariance function K_i is critical for setting the properties of the candidate functions, e.g., smoothness, and consequently for inferring r_i. As our covariance function, we use the following standard squared exponential kernel function, which worked well in our numerical experiments:

$$K_i(x_i, x_j) = \sigma_i^2 \exp \left(-\frac{1}{2} (x_i - x_j)^{\top} L_i^{-1} (x_i - x_j) \right), \tag{14}$$

$\forall x_i, x_j \in \mathbb{R}^{n_u}, \sigma_i > 0$, and $L_i \in \mathbb{R}^{n_u \times n_u}$ is a positive diagonal matrix. Given the past data, the conditional mean and variance of the distribution for $r_i, i = 1, 2, \ldots, n_y$, at an input $\Delta u[k]$, denoted by $\mu_i(\Delta u[k])$ and $\Sigma_i(\Delta u[k])$, respectively, are given by [21]:

$$\mu_i(\Delta u[k]) = C_i \left(\Delta u[k], \Delta \mathbf{u}_{[k-w, k-1]} \right)$$
$$\times \left(C_i \left(\Delta \mathbf{u}_{[k-w, k-1]}, \Delta \mathbf{u}_{[k-w, k-1]} \right) + \sigma_{n,i}^2 I \right)^{-1}$$
$$\times \Delta \mathbf{y}_{[k-w, k-1]}^{(i)}, \tag{15}$$

$$\Sigma_i(\Delta u[k]) = \sigma_i^2 - C_i \left(\Delta u[k], \Delta \mathbf{u}_{[k-w, k-1]} \right)$$
$$\times \left(C_i \left(\Delta \mathbf{u}_{[k-w, k-1]}, \Delta \mathbf{u}_{[k-w, k-1]} \right) + \sigma_{n,i}^2 I \right)^{-1}$$
$$\times C_i \left(\Delta \mathbf{u}_{[k-w, k-1]}, \Delta u[k] \right), \tag{16}$$

where w is the size of the training data,

$$\Delta \mathbf{u}_{[k-w, k-1]} := [\Delta u[k-w], \ldots, \Delta u[k-1]]^{\top}, \tag{17}$$

$$\Delta \mathbf{y}_{[k-w, k-1]}^{(i)} := [\Delta y_i[k-w], \ldots, \Delta y_i[k-1]]^{\top}, \tag{18}$$

$C_i(\Delta \mathbf{u}_{[k-w, k-1]}, \Delta \mathbf{u}_{[k-w, k-1]}) \in \mathbb{R}^{w \times w}$ denotes the covariance matrix as given in (19) as shown at bottom of the next page, $C_i(\Delta u[k], \Delta \mathbf{u}_{[k-w, k-1]}) \in \mathbb{R}^{w}$ denotes the row vector of covariances (kernels) as given in (20) as shown at bottom of the next page,

$$C_i \left(\Delta \mathbf{u}_{[k-w, k-1]}, \Delta u[k] \right) = \left(C_i \left(\Delta u[k], \Delta \mathbf{u}_{[k-w, k-1]} \right) \right)^{\top},$$

$\sigma_{n,i}^2$ is the variance of ϵ_i, denoting the i-th component of ϵ, assumed to be a Gaussian process with zero mean.

The use of Gaussian processes for residual modeling is mathematically equivalent to using a Bayesian linear regression model with (an infinite number of) nonlinear feature vectors; in this case, the posterior distribution over the residuals defined by (15)-(16) can be interpreted as the average of all possible linear regression models with respect to the posterior distribution over the weights. The posterior mean $\mu_i(\Delta u[k])$ gives us an expected value of the residual, $r_i(\Delta u[k])$, whereas the confidence level of the prediction depends on how small the posterior variance $\Sigma_i(\Delta u[k])$ is. Having a high posterior variance implies that $\Delta u[k]$ is substantially different from the previous increments, resulting in a low confidence of the prediction. We intend to exploit such pieces of information provided by the posterior distribution for choosing the control actions.
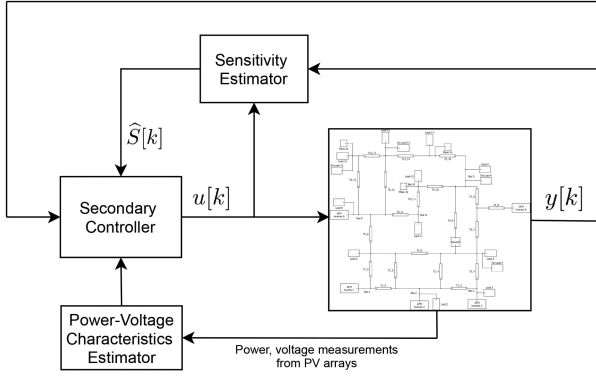
Fig. 1.   Diagram of the proposed data-driven secondary controller.

IV. DATA-DRIVEN SECONDARY CONTROL DESIGN

In this section, we present the secondary controller that relies on the sensitivity-based prediction model and inferred knowledge about the modeling residuals for regulating the system output to the nominal value, and the learned power-voltage characteristics of the PV arrays for dealing with uncertainty in solar power generation. Figure 1 depicts the block diagram of the proposed controller. The sensitivity estimator in (9) and power-voltage characteristics estimator are executed in parallel with the controller. Specifically, the applied control input adjustment and the measured resulting change in the output, $(\Delta u[k], \Delta y[k])$, are provided to the estimator to further update the sensitivity matrix estimate, $\widehat{S}[k]$, using (9). Measurements of the produced power and terminal voltages at the PV arrays are provided to the power-voltage characteristics estimator. Potentially unsafe control actions, for which predictions are not reliable enough, are excluded from the control action space based on the inferred knowledge about the modeling residuals. We then select persistently exciting safe control actions to learn the sensitivities while minimizing the impact of control excitation on its performance.

A. Feedback Optimization With Persistent Excitation

In the following, we present the secondary controller as a solver of some underlying optimization problem. We begin with the following optimization problem:

$$\underset{\varphi}{\text{minimize}} \quad \|\Delta y^*[k] - \widehat{S}[k]\varphi\|_2^2 + \rho\|\varphi\|_2^2 \qquad (21a)$$

$$\text{subject to} \quad \underline{\Delta u}[k] \leq \varphi \leq \overline{\Delta u}[k], \qquad (21b)$$

where $\rho \geq 0$, $\varphi = [\varphi_1, \varphi_2, \ldots, \varphi_{2n}]^\top$, $\underline{\Delta u}[k] = [\underline{\Delta u_1}[k], \underline{\Delta u_2}[k], \ldots, \underline{\Delta u_{2n}}[k]]^\top$, $\overline{\Delta u}[k] = [\overline{\Delta u_1}[k], \overline{\Delta u_2}[k], \ldots, \overline{\Delta u_{2n}}[k]]^\top$, with $\underline{\Delta u_i}[k]$ and $\overline{\Delta u_i}[k]$ denoting respectively the lower and upper bounds on the active power setpoint adjustment at inverter $i \in \mathcal{V}^{(g)}$ at time instant t_k, and $\underline{\Delta u_{i+n}}[k]$ and $\overline{\Delta u_{i+n}}[k]$ denoting the lower and upper

bounds on the reactive power setpoint adjustment at inverter $i \in \mathcal{V}^{(g)}$ at time instant t_k. The objective is to produce the output change $\widehat{S}[k]\varphi$ that tracks the target $\Delta y^*[k] := y^* - y[k-1]$ while penalizing the control effort. The inequality constraints (21b) are meant for keeping the input adjustments within the incremental capacities of the inverters and inside the linear regime, where the linear prediction model is accurate. To be able to identify the sensitivities, we maintain persistent excitation in the control input adjustments by adding a random signal, denoted by $n[k]$, to the solution of the optimization problem (21), denoted by $\varphi^*[k]$, as follows:

$$\Delta u[k] = \varphi^*[k] + n[k]. \qquad (22)$$

Despite the simplicity of the excitation approach, there exist several challenges in choosing suitable values for $n[k]$. On the one hand, $n[k]$ needs to be large enough in order for its effect to be measurable at the output. On the other hand, if $n[k]$ is too large, the control input adjustments might push the operating point away from the desired one, degrading the controller performance. Even more importantly, (22) does not take into account random variations in $\Delta y^*[k]$, e.g., due to load fluctuations, which can add a significant amount of excitation to $\varphi^*[k]$, making the excitation via the addition of $n[k]$ unnecessary. In what follows, we describe an alternative approach for exciting the secondary control commands, where we make use of the random variations in $\Delta y^*[k]$ as appropriate, and avoid unnecessary excitation that (22) might generate.

Consider the following modification of the optimization problem (21), where we add a random signal, denoted by $w[k]$, to the target $\Delta y^*[k]$:

$$\underset{\varphi}{\text{minimize}} \quad \|\Delta y^*[k] + w[k] - \widehat{S}[k]\varphi\|_2^2 + \rho\|\varphi\|_2^2$$

$$\text{subject to} \quad \underline{\Delta u}[k] \leq \varphi \leq \overline{\Delta u}[k],$$

where

$$w[k] = \begin{cases} 0, & \text{if } \{\Delta y^*[l]\}_{l=1}^k \text{ is persistently exciting,} \\ \text{sampled from } (-\Delta y^*[k])U(0, a_1), & \text{otherwise} \end{cases}$$
$$(23)$$

with $a_1 \in (0,1)$, where $U(a,b)$ denotes the continuous uniform distribution over the interval (a,b). For the time being, we neglect the inequality constraints in the following discussion. It holds trivially that if $\widehat{S}[k]$ is invertible for all $k \geq 1$, then, adding $w[l]$ to the target $\Delta y^*[l]$ will generate persistently exciting sequence $\{\varphi^*[l]\}_{l=1}^k$. However, if $\widehat{S}[k]$ has more columns than rows, then, adding $w[k]$ will provide excitation in the subspace that is orthogonal to the null space of $\widehat{S}[k]$. This opens up the possibility of the sequence $\{\varphi^*[l]\}_{l=1}^k$ not being persistently exciting. To rule out such possibility, we excite the control input adjustments as follows:

$$\Delta u[k] = \varphi^*[k], \qquad (24)$$

$$\left[C_i\left(\Delta \mathbf{u}_{[k-w,k-1]}, \Delta \mathbf{u}_{[k-w,k-1]}\right)\right]_{lj} := K_i\left(\Delta u[k-w+l-1], \Delta u[k-w+j-1]\right) \qquad (19)$$

$$\left[C_i\left(\Delta u[k], \Delta \mathbf{u}_{[k-w,k-1]}\right)\right]_j := K_i\left(\Delta u[k], \Delta u[k-w+j-1]\right) \qquad (20)$$

if $\{\Delta u[l]\}_{l=1}^{k}$ is persistently exciting, and

$$\Delta u[k] = \varphi^*[k] + \alpha[k]\nu[k], \tag{25}$$

otherwise, where $\nu[k] \in \mathbb{R}^{2n}$ and $\alpha[k] \in \mathbb{R}$ are randomly chosen such that $\nu[k] \in \text{Null}(\widehat{S}[k])^2$ and

$$\underline{\Delta u}[k] \leq \varphi^*[k] + \alpha[k]\nu[k] \leq \overline{\Delta u}[k]. \tag{26}$$

Since $\widehat{S}[k]\nu[k] = 0$, we note that the perturbation $\alpha[k]\nu[k]$ does not affect the predicted output change, $\widehat{S}[k]\varphi^*[k]$. Hence, if the prediction model is accurate, we expect the perturbation not to have any effect on the system output.

Next, we discuss the control excitation taking into account the inequality constraints. The inequality constraints might become active if the target $\Delta y^*[k]$ is sufficiently large. As a result, the control input adjustments may not be excitable without violating the inequality constraints, namely, there might not exist non-zero $\alpha[k]$ such that (26) holds. To guard against such possibility, we keep the control input adjustments persistently exciting by randomly varying the lower and upper bounds of the constraints in (21b), yielding the following optimization problem:

$$\underset{\varphi}{\text{minimize}} \quad \|\Delta y^*[k] + w[k] - \widehat{S}[k]\varphi\|_2^2 + \rho\|\varphi\|_2^2 \tag{27a}$$

$$\text{subject to} \quad \underline{\Delta u}[k] + \eta_1[k] \leq \varphi \leq \overline{\Delta u}[k] - \eta_2[k], \tag{27b}$$

where $\eta_1[k]$ is sampled from $U(0, a_2|\underline{\Delta u}[k]|)$, $\eta_2[k]$ is sampled from $U(0, a_2|\overline{\Delta u}[k]|)$, with $a_2 \in (0,1)$, at time instant t_k. The setpoints $u[k]$ are adjusted using (24)-(26) based on the solution of (27). Note that if all inequality constraints are active at the solution, then, the approach is equivalent to (22). On the other hand, if only a subset of the inequality constraints are active, then, the target $\Delta y^*[k]$ plays a non-negligible role in exciting the solution $\varphi^*[k]$.

B. Safe Secondary Control

Predictions made by the sensitivity-based prediction model (5) can become less accurate, as a result of large disturbances or lack of control excitation, causing the controller to take unsafe actions. In order to achieve a safer operation, we propose to incorporate the inferred knowledge about the modeling residuals (12) into the optimization (27) as follows:

$$\underset{\varphi}{\text{minimize}} \quad \mathbb{E}\left[\|\Delta y^*[k] + w[k] - \Delta Y_\varphi\|_2^2 + \rho\|\varphi\|_2^2\right] \tag{28a}$$

$$\text{subject to} \quad \Delta Y_\varphi = \widehat{S}[k]\varphi + r(\varphi), \tag{28b}$$

$$\Pr\left(|r_i(\varphi) - \mu_i(\varphi)| \leq \overline{\Delta r_i}\right) \geq \chi, \ i = 1, 2, \ldots, n_y, \tag{28c}$$

$$\underline{\Delta u}[k] + \eta_1[k] \leq \varphi \leq \overline{\Delta u}[k] - \eta_2[k], \tag{28d}$$

where $w[k]$ is given in (23), $r(\varphi) := [r_1(\varphi), r_2(\varphi), \ldots, r_{n_y}(\varphi)]^\top$, $r_i(\varphi) \sim \mathcal{N}(\mu_i(\varphi), \Sigma_i(\varphi))$, with $\mu_i(\varphi)$ and $\Sigma_i(\varphi)$ as defined by (15) and (16), respectively, ΔY_φ denotes the random variable representing the sum of predictions of the sensitivity-based prediction model and the residual prediction model, $\overline{\Delta r_i}$ denotes the prescribed upper bound on the residual

---

^{2}Null(A) denotes the null space of an $a \times b$ matrix A, i.e., Null$(A) := \{x \in \mathbb{R}^b : Ax = 0\}$

r_i's variation from its mean, $\chi \in (0,1)$ is the minimum allowed probability of satisfying the residual constraints. Based on the solution of (28), the setpoints, $u[k]$, are adjusted using (24)-(26). Note that the constraint (28c) excludes those setpoint increments from the control action space for which the prediction errors are highly likely to be large, keeping only those, for which accurate predictions can be made with a high degree of confidence. Since all uncertainties in problem (28) are Gaussian, a deterministic reformulation of (28) can be easily obtained using their moment information; to this end, we write the left-hand side of (28c) as follows:

$$\Pr\left(|r_i(\varphi) - \mu_i(\varphi)| \leq \overline{\Delta r_i}\right)$$

$$= \Pr\left(-\overline{\Delta r_i} \leq r_i(\varphi) - \mu_i(\varphi) \leq \overline{\Delta r_i}\right)$$

$$= \Pr\left(\frac{-\overline{\Delta r_i}}{\Sigma_i^{1/2}(\varphi)} \leq \frac{r_i(\varphi) - \mu_i(\varphi)}{\Sigma_i^{1/2}(\varphi)} \leq \frac{\overline{\Delta r_i}}{\Sigma_i^{1/2}(\varphi)}\right)$$

$$= \Phi\left(\frac{\overline{\Delta r_i}}{\Sigma_i^{1/2}(\varphi)}\right) - \Phi\left(\frac{-\overline{\Delta r_i}}{\Sigma_i^{1/2}(\varphi)}\right)$$

$$= 2\Phi\left(\frac{\overline{\Delta r_i}}{\Sigma_i^{1/2}(\varphi)}\right) - 1, \tag{29}$$

where Φ denotes the cumulative distribution function of the standard normal distribution, in (29) we use the fact that $\Phi(-x) = 1 - \Phi(x)$. Substituting the left-hand side of (28c) with (29), we obtain that

$$2\Phi\left(\frac{\overline{\Delta r_i}}{\Sigma_i^{1/2}(\varphi)}\right) - 1 \geq \chi, \tag{30}$$

from which it follows that

$$\Sigma_i(\varphi) \leq \left(\frac{\overline{\Delta r_i}}{\Phi^{-1}\left(\frac{1+\chi}{2}\right)}\right)^2, \tag{31}$$

because Φ is monotonically increasing. Using the moment information of ΔY_φ, we write the cost (28a) as follows:

$$\mathbb{E}\left[\|\Delta y^*[k] + w[k] - \Delta Y_\varphi\|_2^2 + \rho\|\varphi\|_2^2\right]$$

$$= \|\Delta y^*[k] + w[k] - \widehat{S}[k]\varphi - \mu(\varphi)\|_2^2$$

$$+ \sum_{i=1}^{n_y} \Sigma_i(\varphi) + \rho\|\varphi\|_2^2. \tag{32}$$

By substituting the cost (28a) with (32) and (28c) with (31), we arrive at the following deterministic reformulation of (28):

$$\underset{\varphi}{\text{minimize}} \quad \|\Delta y^*[k] + w[k] - \widehat{S}[k]\varphi - \mu(\varphi)\|_2^2$$

$$+ \sum_{i=1}^{n_y} \Sigma_i(\varphi) + \rho\|\varphi\|_2^2 \tag{33a}$$

$$\text{subject to} \quad \Sigma_i(\varphi) \leq \left(\frac{\overline{\Delta r_i}}{\Phi^{-1}\left(\frac{1+\chi}{2}\right)}\right)^2, \ i = 1, 2, \ldots, n_y, \tag{33b}$$

$$\underline{\Delta u}[k] + \eta_1[k] \leq \varphi \leq \overline{\Delta u}[k] - \eta_2[k]. \tag{33c}$$

Algorithm 1: *Safe Data-Driven Secondary Control With Persistent Excitation.*

1. Initialize $\rho \geq 0$, $a_1 \in (0,1)$, $a_2 \in (0,1)$.
2. If $\{\Delta y^*[l]\}_{l=1}^k$ is persistently exciting:
       set $w[k] = 0$
   else:
       select $w[k] \sim (-\Delta y^*[k])U(0, a_1)$.
   Select $\eta_1[k] \sim U(0, a_2|\underline{\Delta u}[k]|)$,
       $\eta_2[k] \sim U(0, a_2|\overline{\Delta u}[k]|)$.
3. Find a solution of (33), $\varphi^*[k]$.
4. If $\{\Delta u[l]\}_{l=1}^k$ is persistently exciting:
       apply $\Delta u[k] = \varphi^*[k]$
   else:
       choose randomly $\nu[k]$ and $\alpha[k]$ such that:
         $\nu[k] \in \text{Null}(\widehat{S}[k])$ and
         $\underline{\Delta u}[k] \leq \varphi^*[k] + \alpha[k]\nu[k] \leq \overline{\Delta u}[k]$;
       apply $\Delta u[k] = \varphi^*[k] + \alpha[k]\nu[k]$.

Because of the non-convex objective function and constraint (33b), the optimization problem (33) is non-convex, and difficult to solve. However, local optimal solutions can be obtained by utilizing sequential quadratic programming (SQP). The pseudocode for the proposed secondary control approach is provided in Algorithm 1.

C. Safe Secondary Control With PV Power Tracking

In the following, we take into consideration the constraints that PV arrays impose on the secondary controller during its execution. As discussed earlier, to extract a desired amount of power from a PV array, a certain voltage must be applied across its terminals, as determined by its power-voltage characteristic. Hence, the voltage setpoint must be computed so as to allow the PV array to track the secondary control inputs. To this end, we augment the optimization problem (33) with the learned power-voltage characteristics (2) as follows:

$$\underset{\varphi,v}{\text{minimize}} \quad \|\Delta y^*[k] + w[k] - \widehat{S}[k]\varphi - \mu(\varphi)\|_2^2$$

$$+ \sum_{i=1}^{n_y} \Sigma_i(\varphi) + \rho\|\varphi\|_2^2 \tag{34a}$$

$$\text{subject to} \quad \Sigma_i(\varphi) \leq \left(\frac{\overline{\Delta r_i}}{\Phi^{-1}\left(\frac{1+\chi}{2}\right)}\right)^2, \; i = 1, 2, \ldots, n_y, \tag{34b}$$

$$\underline{\Delta u}[k] + \eta_1[k] \leq \varphi \leq \overline{\Delta u}[k] - \eta_2[k], \tag{34c}$$

$$\underline{\Delta u}[k] \leq \varphi + \alpha[k]\nu[k] \leq \overline{\Delta u}[k], \tag{34d}$$

$$c_i(v_i, \beta^{(i)}[k]) = P_i[k-1] + \varphi_i + \alpha_i[k]\nu_i[k], \tag{34e}$$

$$\underline{v}_i \leq v_i \leq \overline{v}_i, \; i \in \mathcal{V}_{pv}, \tag{34f}$$

where we recall that $w[k]$ is given in (23), $\alpha[k] \in \mathbb{R}$, $\eta_1[k]$ is sampled from $U(0, a_2|\underline{\Delta u}[k]|)$, and $\eta_2[k]$ is sampled from
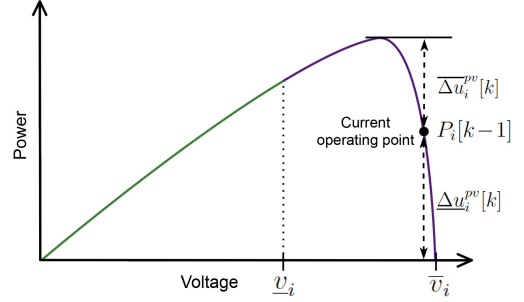

Fig. 2. Illustration of the relaxation of the power-voltage characteristic (34e) subject to an interval voltage constraint (34f) to the interval power constraint based on the incremental capacities of a PV array with respect to the current operating point.

$U(0, a_2|\overline{\Delta u}[k]|)$, $v = [v_1, v_2, \ldots, v_{|\mathcal{V}_{pv}|}]^\top$, $c_i(v_i, \beta^{(i)}[k])$ represents the estimated power-voltage characteristic of the PV array i, with $\beta^{(i)}[k] = [\beta_0^{(i)}[k], \beta_2^{(i)}[k], \ldots, \beta_{2d}^{(i)}[k]]^\top$ denoting the estimated coefficients of the fitted polynomial model, $\underline{v}_i$ and $\overline{v}_i$ denote the lower and upper bounds on the voltage applied across the terminals of the PV array $i \in \mathcal{V}_{pv}$, and $P_i[k-1] := P_i(t_k^-)$, with $P_i(t)$ denoting the active power injection by the PV array $i \in \mathcal{V}_{pv}$ at time t. The constraint (34e) serves to maintain a power balance between the generated solar power and the inverter active power output, while neglecting the inverter losses. Note that we have integrated step 4 of Algorithm 1 directly into the optimization (34), where $\alpha[k] = 0$, if $\{\Delta u[l]\}_{l=1}^{k-1}$ is persistently exciting, and $\alpha[k]$ is randomly chosen, otherwise. Let $(\varphi^*[k], v^*[k])$ denote a solution of (34), where $\varphi^*[k]$ and $v^*[k]$ are vectors of optimal power setpoint increments and voltage setpoints, respectively. We can further simplify the nonlinear power-voltage characteristics in (34e) but still recover $(\varphi^*[k], v^*[k])$. To this end, as illustrated in Fig. 2, we can replace the power-voltage characteristics (34e) and interval voltage constraints (34f) with the interval power constraints to keep the active power setpoint increments within the incremental capacities of the PV arrays with respect to the current operating point. This yields the following simpler optimization problem over only power setpoint increments:

$$\underset{\varphi}{\text{minimize}} \quad \|\Delta y^*[k] + w[k] - \widehat{S}[k]\varphi - \mu(\varphi)\|_2^2$$

$$+ \sum_{i=1}^{n_y} \Sigma_i(\varphi) + \rho\|\varphi\|_2^2 \tag{35a}$$

$$\text{subject to} \quad \Sigma_i(\varphi) \leq \left(\frac{\overline{\Delta r_i}}{\Phi^{-1}\left(\frac{1+\chi}{2}\right)}\right)^2, \; i = 1, 2, \ldots, n_y, \tag{35b}$$

$$\underline{\Delta u}[k] + \eta_1[k] \leq \varphi \leq \overline{\Delta u}[k] - \eta_2[k], \tag{35c}$$

$$\underline{\Delta u}[k] \leq \varphi + \alpha[k]\nu[k] \leq \overline{\Delta u}[k], \tag{35d}$$

$$\underline{\Delta u_i^{pv}}[k] \leq \varphi_i + \alpha_i[k]\nu_i[k] \leq \overline{\Delta u_i^{pv}}[k], \; i \in \mathcal{V}_{pv}, \tag{35e}$$

where $\overline{\Delta u_i^{pv}}[k] = \overline{p}_i[k] - P_i[k-1]$, and $\underline{\Delta u_i^{pv}}[k] = \underline{p}_i[k] - P_i[k-1]$ denote the maximum and minimum incremental capacities of the PV array i,

and $\quad \underline{p}_i[k] = \min_{\underline{v}_i \le v_i \le \overline{v}_i} c_i(v_i, \beta^{(i)}[k]) \quad$ and $\quad \overline{p}_i[k] = \max_{\underline{v}_i \le v_i \le \overline{v}_i} c_i(v_i, \beta^{(i)}[k])$ denote the estimates of the minimum and maximum active power capacity of the PV array i for terminal voltages from the interval $[\underline{v}_i, \overline{v}_i]$; the estimates $\underline{p}_i[k]$ and $\overline{p}_i[k]$ can be easily obtained from the learned power-voltage characteristic of the PV array i because of its concavity properties; see Fig. 2 for a graphical depiction.

In (35), we are content with finding the power setpoints that are to be tracked by the PV arrays given their limited incremental capacities. Since, as illustrated in Fig. 2, the interval power constraints (35e) include all possible power outputs of the PV arrays when they are operated within the interval voltage constraints (34f), solving (35) will give us the optimal power setpoint increments, $\varphi^*[k]$. To get $v^*[k]$, we need to separately solve (34e) by substituting $\varphi^*[k]$ for φ, e.g., by means of the power tracking algorithm in [19, Algorithm 2]. This algorithm uses a Newton's method to first find a point on the power-voltage curve that has a negative slope and power greater than the power setpoint; then, it adjusts voltage until power becomes close enough to the power setpoint.

Inclusion of the inequality constraints in (35e) may lead to a lack of persistent excitation of the control inputs. Similar to (27), to guard against such possibility, we randomly vary the lower and upper bounds of the constraints in (35e) yielding the following optimization problem for safe secondary control:

$$\text{minimize}_{\varphi} \quad \|\Delta y^*[k] + w[k] - \widehat{S}[k]\varphi - \mu(\varphi)\|_2^2$$

$$+ \sum_{i=1}^{n_y} \Sigma_i(\varphi) + \rho\|\varphi\|_2^2 \tag{36a}$$

$$\text{subject to} \quad \Sigma_i(\varphi) \le \left(\frac{\overline{\Delta r_i}}{\Phi^{-1}\left(\frac{1+\chi}{2}\right)}\right)^2, \quad i = 1, 2, \dots, n_y, \tag{36b}$$

$$\underline{\Delta u}[k] + \eta_1[k] \le \varphi \le \overline{\Delta u}[k] - \eta_2[k], \tag{36c}$$

$$\underline{\Delta u}[k] \le \varphi + \alpha[k]\nu[k] \le \overline{\Delta u}[k], \tag{36d}$$

$$\underline{\Delta u}_i^{pv}[k] + \underline{\zeta}_i[k] \le \varphi_i + \alpha_i[k]\nu_i[k], \quad i \in \mathcal{V}_{pv},$$

$$\varphi_i + \alpha_i[k]\nu_i[k] \le \overline{\Delta u}_i^{pv}[k] - \overline{\zeta}_i[k], \tag{36e}$$

where $\underline{\zeta}_i[k] = 0$, if $\{\underline{\Delta u}^{pv}[l]\}_{l=1}^k$ is persistently exciting, and $\underline{\zeta}_i[k] \sim U(0, a_3|\underline{\Delta u}_i^{pv}[k]|)$, otherwise, with $a_3 \in (0, 1)$, at time instant t_k; $\overline{\zeta}_i[k] = 0$, if $\{\overline{\Delta u}^{pv}[l]\}_{l=1}^k$ is persistently exciting, and $\overline{\zeta}_i[k] \sim U(0, a_3|\overline{\Delta u}_i^{pv}[k]|)$, otherwise. In Algorithm 2, we provide the pseudocode for the proposed approach combining the secondary control objectives with the PV power tracking objectives.

V. NUMERICAL SIMULATIONS

In this section, we showcase the proposed secondary controller using a modified version of the IEEE-14 bus test system [22], with energy sources providing both active and reactive power at buses 1, 2, 3, and reactive power sources at buses 6 and 8 replaced by inverter-interfaced DERs, as described in the single line diagram of the test system in Figure 3. We also compare the
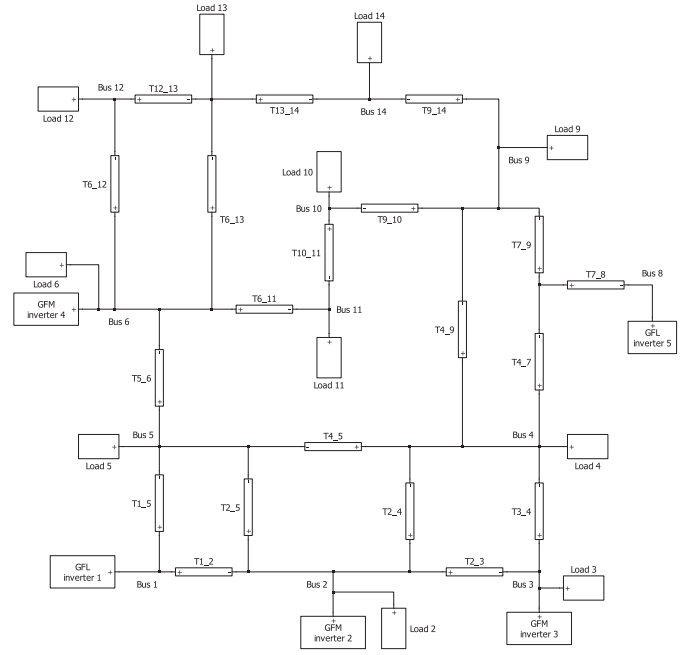
Fig. 3. The single line diagram of the modified IEEE-14 bus test system.

Algorithm 2: Safe Data-Driven Secondary Control With PV Power Tracking.

1. Initialize $\rho \ge 0$, $a_1 \in (0, 1)$, $a_2 \in (0, 1)$, $a_3 \in (0, 1)$.
2. Set
   - $w[k] = 0$, if $\{\Delta y^*[l]\}_{l=1}^k$ is persistently exciting, and $w[k] \sim (-\Delta y^*[k])U(0, a_1)$, otherwise;
   - $\eta_1[k] \sim U(0, a_2|\underline{\Delta u}[k]|)$; $\eta_2[k] \sim U(0, a_2|\overline{\Delta u}[k]|)$;
   - $\underline{\zeta}_i[k] = 0$, if $\{\underline{\Delta u}^{pv}[l]\}_{l=1}^k$ is persistently exciting, and $\underline{\zeta}_i[k] \sim U(0, a_3|\underline{\Delta u}_i^{pv}[k]|)$, otherwise;
   - $\overline{\zeta}_i[k] = 0$, if $\{\overline{\Delta u}^{pv}[l]\}_{l=1}^k$ is persistently exciting, and $\overline{\zeta}_i[k] \sim U(0, a_3|\overline{\Delta u}_i^{pv}[k]|)$, otherwise;
   - $\alpha[k] = 0$, if $\{\Delta u[l]\}_{l=1}^{k-1}$ is persistently exciting, and $\alpha[k]$ is randomly chosen, otherwise;
   - $\nu[k]$ is randomly chosen such that $\nu[k] \in \text{Null}(\widehat{S}[k])$.
3. Apply $\Delta u[k] = \varphi^*[k]$, a solution of (36).
4. Compute $v_i^*[k]$ such that $c_i(v_i^*[k], \beta^{(i)}[k]) = P_i[k-1] + \varphi_i^*[k] + \alpha_i[k]\nu_i[k]$, $i \in \mathcal{V}_{pv}$, by using [19, Algorithm 2].

---

performance of the proposed approach with that of an existing one.

A. Case Study

We apply Algorithm 2 to regulate system frequency and voltage magnitudes at buses 4, 9, 12 to the corresponding nominal values, namely, 60 Hz, $V_4^* = 1.02$ pu, $V_9^* = 1$ pu, and $V_{12}^* = 1$ pu, respectively. The GFM-inverter-interfaced DERs are located at buses 2, 3 and 6, and the GFL inverters interfacing PV arrays are located at buses 1 and 8. The DER index sets are given by: $\mathcal{V}_{pv} = \{1, 5\}$, and $\mathcal{V}^{(I)} = \{2, 3, 4\}$. PV generation is
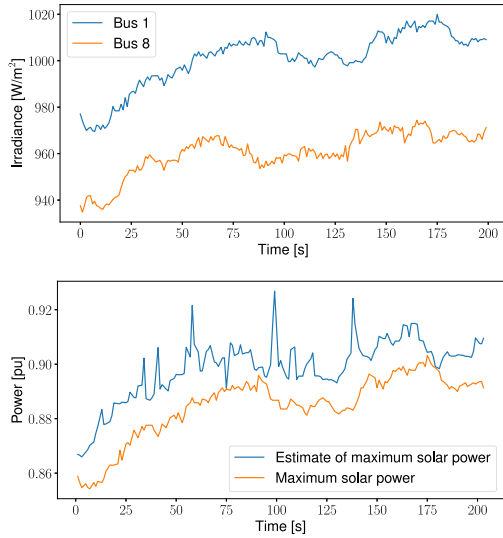
Fig. 4. Solar irradiance profile at buses 1 and 8, maximum available solar power at bus 1 and its estimate.

Fig. 5. Trajectories of system frequency, and voltage magnitudes at buses 4, 9, and 12.

simulated at buses 1 and 8 using solar irradiance data collected from NREL's Oahu Solar Measurement Grid [23] on Oct 1, 2011, from 11:55:00 am to 12:01:40 pm; see Figure 4. As described in Section II-C, the estimation of the power-voltage characteristics of the PV arrays at buses 1 and 8 is performed by fitting the polynomial models in (2), with $d = 4$, to the collected power-voltage measurements $\{(v_1[l], p_1[l])\}_{l=k-w}^{k}$ and $\{(v_5[l], p_5[l])\}_{l=k-w}^{k}$, with $w = 9$. Figure 4 also shows the maximum available solar power at bus 1 and its estimate obtained from the learned power-voltage characteristics.

Load perturbations occur every 4 s, and the secondary controller is executed every 1 s except for the time instants when the loads are perturbed. This separation between the controller actions and load changes is introduced to clearly demonstrate the effectiveness of the control approach. Otherwise, if the loads change while the system is settling down after a secondary controller execution, it is more challenging to evaluate the controller performance and the accuracy of the prediction model.

We use the following values to initialize the parameters of Algorithm 2: $\rho = 0$, $a_1 = 0.5$, $a_2 = 0.4$, $\underline{\Delta u_i}[k] = -0.1$ pu, $\overline{\Delta u_i}[k] = 0.1$ pu, $i \in \mathcal{V}^{(g)}$, and $\alpha[k] \sim U(0, 0.05)$. The parameters of the kernel function are as follows: $\sigma_i^2 = 10^{-5}$, $L_i = 0.025$, $i = 1, 2, \ldots, n_y$. As regards the probabilistic constraints in (36b), we set the values of the parameters defining them as follows: $\chi = 0.9$, $\overline{\Delta r_i} = 4 \times 10^{-3}$. The feedback optimization problem (36) is solved using SQP on CVXPY [24]. The sensitivity estimator in (9) is executed in parallel with the controller. Specifically, the applied control input adjustment and the measured resulting change in the output, $(\Delta u[k], \Delta y[k])$, are provided to the estimator to further update the sensitivity matrix estimate, $\widehat{S}[k]$, using (9). We use the following values to initialize the estimator parameters in (9): $\lambda = 0.995$, and $\gamma = 10^{-3}$.

Figure 5 shows the steady-state values of system frequency and voltage magnitudes at buses 4, 9, 12 after each load perturbation, and after each secondary control action. [Note that three control actions are taken before another load perturbation occurs.] It can be seen that the control actions determined by
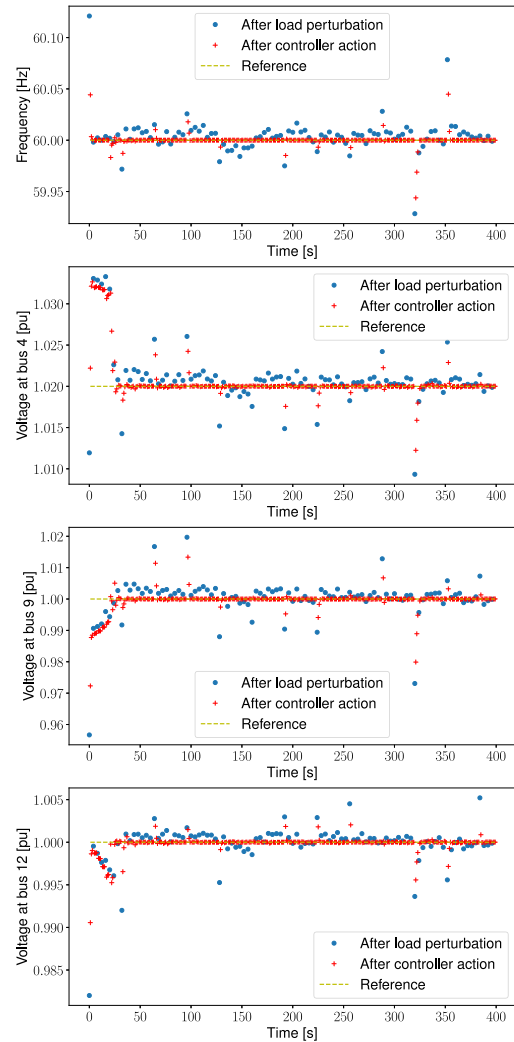
Algorithm 2 manage to keep the system output close to the nominal values despite the system experiencing significant load variations.

Figure 6 shows the evolution of the sensitivity estimates corresponding to system frequency, and actual sensitivities. It can be seen that the sensitivity estimates are very close to the actual values, and that negligible differences still exist between them, since the sensitivity estimation via ridge regression (10) is biased due to the use of regularization. During the first 20 s, the sensitivity estimates experience some transients quickly reaching a steady state. Also note that the active power setpoint adjustments, $\Delta P^r[k]$, have much more significant effect on the frequency than the reactive power setpoint adjustments, $\Delta Q^r[k]$, which is consistent with the inductive nature of the test system network. Figure 6 also shows the predictions of system frequency, where each prediction is given by the sum of the prediction made by the sensitivity-based prediction model (5) and the correction equal to the posterior mean of the residual (15). Prediction errors are less than 10 % in 90 % of all test
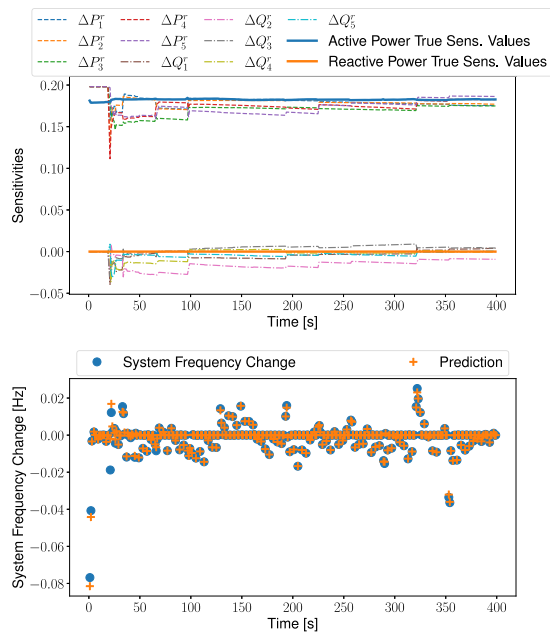
Fig. 6. Evolution of the estimated sensitivities corresponding to system frequency, and the actual sensitivity values, and predictions of the frequency changes.

cases, where the prediction errors are computed as follows:

$$e_i[k] = \frac{|\Delta y_i[k] - \widehat{\Delta y_i}[k]|}{\max(|\Delta y_i[k]|, \overline{y}_{m,i})} 100\%,$$

where $e_i[k]$ is the prediction error corresponding to the output change $\Delta y_i[k]$, $\overline{y}_{m,i}$ is the threshold below which the changes in the output y_i are not measurable. For example, for system frequency, we set $\overline{y}_{m,1} = 10^{-4}$ Hz. We note that the predictions are less accurate during the initial transient period, when the operating point changes significantly, or when the control input adjustments are too large going over the linear regime of the prediction model.

B. Comparative Study

Figure 7 compares the performance of our approach with that of the existing two-stage voltage control approach proposed in [25]. This approach was developed to maintain the voltage magnitudes at buses 4, 9, and 12 between the operational lower and upper bounds, both chosen in this example to be equal to the voltage setpoints. Similar to our approach, it only uses the voltage magnitude measurements of the buses it aims to regulate. As can be seen in Figure 7, our approach significantly outperforms the two-stage voltage control approach, which is unable to keep the voltage magnitudes precisely at their setpoints, but only within a certain error.

C. Benefits of Residual Inference for Secondary Control

Figure 8 shows scatterplots of the predicted standard deviation of the posterior residual distribution and prediction errors for two cases: with and without using the inferred knowledge about the residuals in secondary control. As can be seen in Fig 8, there
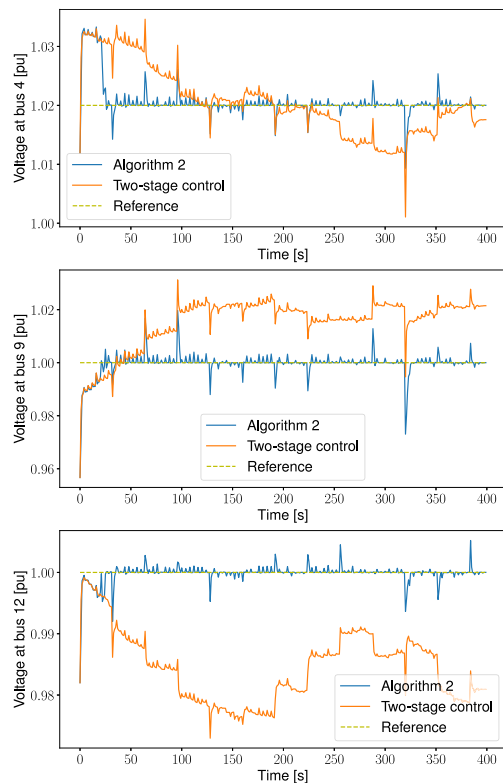

Fig. 7. Trajectories of the voltage magnitudes at buses 4, 9, and 12 for Algorithm 2 and two-stage voltage control approach [25].
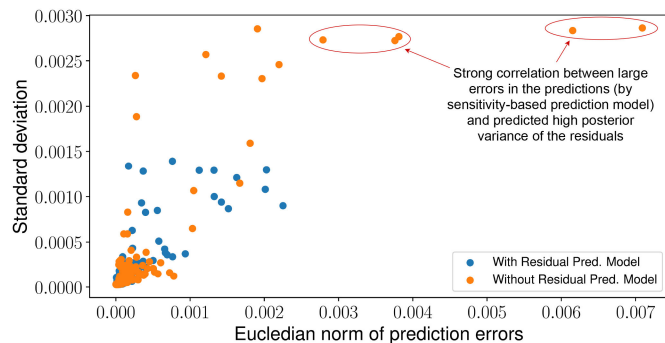

Fig. 8. Predicted standard deviation of the posterior residual distribution and prediction errors for two cases: with and without using the inferred knowledge about the residuals in secondary control.

is a strong correlation between large prediction errors and high posterior residual variance, enabling the controller to find safe control actions with smaller posterior residual variance, which consequently decreases prediction uncertainties and improves accuracy. This demonstrates the advantages of using the learned posterior distribution of the residuals to perform secondary control more cautiously.

VI. CONCLUSION

In this paper, we developed a data-driven secondary controller for power networks with a deep penetration of GFM inverters. The controller chooses safe control actions (in the sense of

ensuring operational reliability is maintained) based on the learned power system sensitivities, e.g., of system frequency to the inverter setpoints, and posterior distribution of the modeling residuals used to correct the predictions of the sensitivity-based prediction model and provide information about their confidence level. To be able to learn a useful prediction model, we presented an approach to keep the control inputs persistently exciting without significantly degrading the controller performance.

REFERENCES

[1] K. Zhou, C. Fu, and S. Yang, "Big data driven smart energy management: From big data to big insights," *Renewable Sustain. Energy Rev.*, vol. 56, pp. 215–225, 2016.

[2] C. De Persis and P. Tesi, "Formulas for data-driven control: Stabilization, optimality, and robustness," *IEEE Trans. Autom. Control*, vol. 65, no. 3, pp. 909–924, Mar. 2020.

[3] O. Nelles, *Nonlinear System Identification*, 2nd ed. Berlin, Germany: Springer Int. Publishing, 2020.

[4] Y. C. Chen, A. D. Domínguez-García, and P. W. Sauer, "Measurement-based estimation of linear sensitivity distribution factors and applications," *IEEE Trans. Power Syst.*, vol. 29, no. 3, pp. 1372–1382, May 2014.

[5] K. E. Van Horn, A. D. Domínguez-García, and P. W. Sauer, "Measurement-based real-time security-constrained economic dispatch," *IEEE Trans. Power Syst.*, vol. 31, no. 5, pp. 3548–3560, Sep. 2016.

[6] H. Zhang, J. Zhou, Q. Sun, J. M. Guerrero, and D. Ma, "Data-driven control for interlinked ac/dc microgrids via model-free adaptive control and dual-droop control," *IEEE Trans. Smart Grid*, vol. 8, no. 2, pp. 557–571, Mar. 2017.

[7] Z. Yan and Y. Xu, "Data-driven load frequency control for stochastic power systems: A deep reinforcement learning method with continuous action search," *IEEE Trans. Power Syst.*, vol. 34, no. 2, pp. 1653–1656, Mar. 2019.

[8] P. Hidalgo-Gonzalez, R. Henriquez-Auba, D. S. Callaway, and C. J. Tomlin, "Frequency regulation using data-driven controllers in power grids with variable inertia due to renewable energy," in *Proc. IEEE Power Energy Soc. Gen. Meeting*, 2019, pp. 1–5.

[9] H. Xu, A. D. Domínguez-García, and P. W. Sauer, "Data-driven coordination of distributed energy resources for active power provision," *IEEE Trans. Power Syst.*, vol. 34, no. 4, pp. 3047–3058, Jul. 2019.

[10] S. Karagiannopoulos, R. Dobbe, P. Aristidou, D. Callaway, and G. Hug, "Data-driven control design schemes in active distribution grids: Capabilities and challenges," in *Proc. IEEE PowerTech*, 2019, pp. 1–6.

[11] H. Xu, A. D. Domínguez-García, V. V. Veeravalli, and P. W. Sauer, "Data-driven voltage regulation in radial power distribution systems," *IEEE Trans. Power Syst.*, vol. 35, no. 3, pp. 2133–2143, May 2020.

[12] S. S. Madani, C. Kammer, and A. Karimi, "Data-driven distributed combined primary and secondary control in microgrids," *IEEE Trans. Control Syst. Technol.*, vol. 12, no. 3, pp. 1340–1347, 2020.

[13] Y. Chen, Y. Shi, and B. Zhang, "Data-driven optimal voltage regulation using input convex neural networks," *Electric Power Syst. Res.*, vol. 189, 2020, Art. no. 106741.

[14] Q. Yang, G. Wang, A. Sadeghi, G. B. Giannakis, and J. Sun, "Two-timescale voltage control in distribution grids using deep reinforcement learning," *IEEE Trans. Smart Grid*, vol. 11, no. 3, pp. 2313–2323, May 2020.

[15] R. Dobbe, O. Sondermeijer, D. Fridovich-Keil, D. Arnold, D. Callaway, and C. Tomlin, "Toward distributed energy services: Decentralizing optimal power flow with machine learning," *IEEE Trans. Smart Grid*, vol. 11, no. 2, pp. 1296–1306, Mar. 2020.

[16] R. Dobbe *et al.*, "Learning to control in power systems: Design and analysis guidelines for concrete safety problems," *Electric Power Syst. Res.*, vol. 189, 2020, Art. no. 106615.

[17] Y. Xu, Z. Qu, R. Harvey, and T. Namerikawa, "Data-driven wide-area control design of power system using the passivity shortage framework," *IEEE Trans. Power Syst.*, vol. 36, no. 2, pp. 830–841, Mar. 2021.

[18] K. J. Åström and B. Wittenmark, *Adaptive Control: SecEdition*. Mineola, New York, NY, USA: Dover, 2008.

[19] X. Zhang, V. Purba, M. Hong, and S. Dhople, "A sum-of-squares optimization method for learning and controlling photovoltaic systems," in *Proc. Amer. Control Conf.*, 2020, pp. 2376–2381.

[20] M. Lu, S. Dutta, V. Purba, S. Dhople, and B. Johnson, "A grid-compatible virtual oscillator controller: Analysis and design," in *Proc. IEEE Energy Convers. Congr. Expo.*, 2019, pp. 2643–2649.

[21] C. E. Rasmussen and C. K. I. Williams, *Gaussian Processes for Machine Learning*. Cambridge, MA, USA: MIT Press, 2006.

[22] *IEEE 14-Bus System, Power Systems Test Case Archive*, [Online] Available: https://www.ece.uw.edu/research/pstca/pf14/pg_tca14bus.htm.

[23] M. Sengupta and A. Andreas, "Oahu solar measurement grid (1-Year archive): 1-Second solar irradiance; Oahu, Hawaii (Data)," NREL Rep. DA-5500-56506, 2010.

[24] S. Diamond and S. Boyd, "CVXPY: A python-embedded modeling language for convex optimization," *J. Mach. Learn. Res.*, vol. 17, no. 83, pp. 1–5, 2016.

[25] B. A. Robbins, C. N. Hadjicostis, and A. D. Domínguez-García, "A two-stage distributed architecture for voltage control in power distribution systems," *IEEE Trans. Power Syst.*, vol. 28, no. 2, pp. 1470–1482, May 2013.

Madi Zholbaryssov received the B.S., M.S., and Ph.D. degrees in electrical engineering from the University of Illinois at Urbana-Champaign, Champaign, IL, USA, in 2011, 2014, and 2019, respectively. He is currently a Postdoctoral Research Associate with the Department of Electrical and Computer Engineering, University of Illinois at Urbana-Champaign. His current research interests include applications of distributed control and optimization in electric power systems.

Alejandro D. Domínguez-García (Senior Member, IEEE) received the Electrical Engineering degree from the University of Oviedo, Oviedo, Spain, in 2001 and the Ph.D. degree in electrical engineering and computer science from the Massachusetts Institute of Technology, Cambridge, MA, USA, in 2007. He is currently a Professor with the Department of Electrical and Computer Engineering (ECE), and Research Professor with the Coordinated Science Laboratory and the Information Trust Institute, University of Illinois at Urbana-Champaign. He is affiliated with the ECE Power and Energy Systems area, and since August 2011, has been a Grainger Associate. His research interests include system reliability theory and control, and their applications to electric power systems, power electronics, and embedded electronic systems for safety-critical or fault-tolerant aircraft, aerospace, and automotive applications. Dr. Domínguez-García was the recipient of the NSF CAREER Award in 2010, the Young Engineer Award from the IEEE Power and Energy Society in 2012, and the U of I College of Engineering Dean's Award for Excellence in Research in 2015. In 2014, he was invited by the National Academy of Engineering to attend the US Frontiers of Engineering Symposium, and was selected by the University of Illinois at Urbana-Champaign Provost to receive a Distinguished Promotion Award.

He is currently the Editor of the IEEE TRANSACTIONS ON POWER SYSTEMS and IEEE TRANSACTIONS ON CONTROL OF NETWORK SYSTEMS. From 2011 to 2017, he was also the Editor of the IEEE POWER ENGINEERING LETTERS.